

# Improved Thermal Management of H<sub>2</sub>O<sub>2</sub> Decomposition with Microreactors for a SOFC Oxidant Source aboard Unmanned Undersea Vehicles

*E. Lennon<sup>1</sup>, A. A. Burke<sup>2</sup>, and R. S. Besser<sup>1</sup>*

*1. Stevens Institute of Technology, Hoboken, NJ 07030 (elennon@stevens.edu, rbesser@stevens.edu)*

*2. Naval Undersea Warfare Center, Newport, RI 02841*

## Abstract

The catalytic decomposition of hydrogen peroxide (H<sub>2</sub>O<sub>2</sub>) into water (H<sub>2</sub>O) and oxygen (O<sub>2</sub>) [H<sub>2</sub>O<sub>2</sub> → H<sub>2</sub>O + ½ O<sub>2</sub>] is notoriously susceptible to thermal runaway (Heat of Reaction: -98 kJ/mol). However, liquid H<sub>2</sub>O<sub>2</sub> has high oxygen density making it a particularly attractive oxidant for applications where air-independence and space limitations elicit additional power supply design challenges. Microchemical technologies have intrinsically higher surface-to-volume ratios (SV) potentially facilitating heat and mass transfer. This study investigated a micro-scale reactor to illustrate thermal management and assess oxygen production during the multiphase decomposition of H<sub>2</sub>O<sub>2</sub> as an oxidant for an unmanned undersea vehicle (UUV) solid oxide fuel cell (SOFC). A microscale packed bed (MPB) reactor model with channel radius 0.5 mm was developed in the finite element modeling program COMSOL. The properties of the multiphase product stream were described by weighted averages of the component species under the assumption of a well-mixed, dispersed phase. The micro-scale channel alone (SV: 2254 m<sup>2</sup>/m<sup>3</sup>) failed to prevent significant heat rise during simulated decomposition in the convectively cooled reactor channel (T<sub>rise</sub> ~ 100 K). The extension of surface area around the reactor channel (SV: 188,439 m<sup>2</sup>/m<sup>3</sup>) improved passive cooling, resulting in simulated MPB temperature rises less than 7 K and experimental MPB temperature rises less 4 K. Decomposition was also tested using a second miniature tubular, catalyst-coated (TCC) reactor model with channel radius of 1.5 mm (SV: 2666 m<sup>2</sup>/m<sup>3</sup>) for thermal comparison with the MPB. Experimental data collected with the MPB reactor were compared to the numerical MPB models. Pulsating oxygen production, consistent with two-phase slug flow, was observed at the outlet of the MPB reactor over flow rates of 0.05 and 0.15 ml/min. Although slug flow was not specifically accounted for in the model, the time-averaged empirical behavior compared well to the simulated behavior for the MPB. Thermal management of the MPB was found to be superb and clearly superior to that of the miniature scale TCC. Overall these results showed the feasibility of oxygen generation and improved thermal control during H<sub>2</sub>O<sub>2</sub> decomposition with a microchemical approach relative to conventionally-sized or even miniature (mm-scale) reactors.

## Introduction

A major challenge facing the design of air-independent power systems is continuous energy generation. High energy density and potentially low operating costs make fuel cells an attractive option for high endurance, undersea vehicle applications [1]. However, undersea fuel cell power systems require an oxidant supply. Hydrogen peroxide (H<sub>2</sub>O<sub>2</sub>) readily decomposes into water (H<sub>2</sub>O) and oxygen (O<sub>2</sub>) [H<sub>2</sub>O<sub>2</sub> → H<sub>2</sub>O + ½ O<sub>2</sub>] upon contact with a number of commercially available metal catalysts offering a dense source of oxygen per unit volume that makes it a valuable commodity as an air-independent fuel cell oxidant [2]. Kinetic experiments have shown manganese dioxide (MnO<sub>2</sub>) is an effective and inexpensive H<sub>2</sub>O<sub>2</sub> decomposition catalyst with reported activation energies ranging

from 20 to 44 kJ/mole [3]. Furthermore, the high oxygen density, ease of handling, and commercial infrastructure of  $H_2O_2$  add to its appeal as an oxidant source [4].

Despite these advantages, it is well established that catalytic  $H_2O_2$  decomposition is highly exothermic, which has historically limited its application as a power system oxidant, especially within the US Navy community [5]. In addition, like other exothermic multiphase reactions, the liquid and gas product stream from  $H_2O_2$  decomposition can lead to undesirable pressure increases and an irregular distribution of thermal capacity in conventionally sized reactors promoting hot spots and the possibility of thermal runaway [6]. Microscale (relevant fluid dimension in subunits  $< 1$  mm) chemical systems by virtue of small-scale geometry, possess high surface-to-volume ratios resulting in heat and mass transfer coefficients capable of inhibiting thermal runaway. Conventional reactors have surface to volume ratios of  $10^2$   $m^2/m^3$ , whereas small-scale reactors possess surface-to-volume ratios that are at least an order of magnitude greater [7]. The microscale packed bed (MPB) microreactor and tubular catalyst coated (TCC) reactor used in this research had surface-to-volume ratios of  $1.8 \times 10^5$   $m^2/m^3$  and  $2.6 \times 10^3$   $m^2/m^3$  respectively. Although laminar flow is typical in many homogeneously dispersed product streams within microchannels [8], slug flow may also develop. One study presented two phase flow evolution of  $O_2$  gas bubbles and liquid water from platinum catalyzed  $H_2O_2$  decomposition in 80  $\mu m$  diameter microchannels in three stages: liquid decomposition, bubble coalescence, and bubble slug [9]. Despite the complexities of the multiphase product stream generated from  $H_2O_2$  decomposition, this work aimed to demonstrate thermal management feasibility and assess  $O_2$  production during the catalytic multiphase decomposition of  $H_2O_2$  of the MPB reactor.

## Methods

### *Simulated $H_2O_2$ Decomposition*

#### *I. Model Geometries*

Figure 1A shows the MPB channel with a height of 0.5 mm and length of the 5 cm. Surrounding the MPB channel was a rectangular stainless steel 316 block (7x2x0.4 cm). A Plexiglas (PMMA) cover (7x2x0.1 cm) served as the reactor seal. Shown in Figure 1B is the TCC geometry and dimensions in cm used for thermal comparison with the MPB.

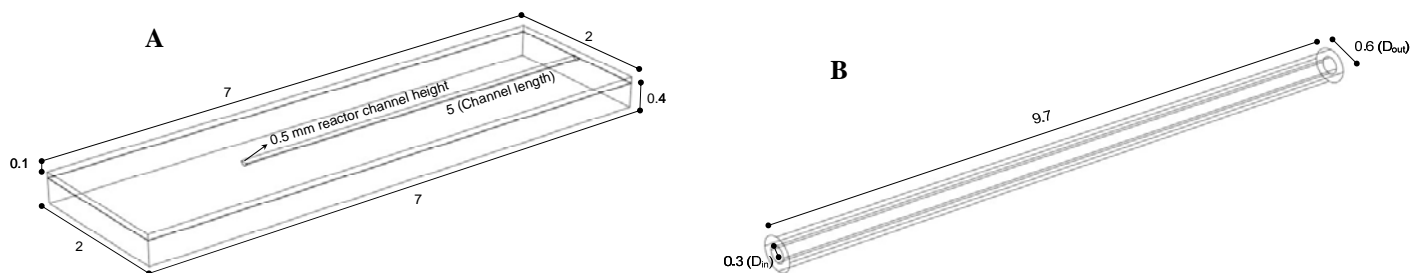


Figure 1A and 1B: MPB Model Geometry and TCC model geometry. All dimensions in cm except where noted.

## II. Balance Equations and Assumptions

Mass Balance. Assumptions pertaining to the phases of the reactant and product species of the mass balance were made. The amount of H<sub>2</sub>O<sub>2</sub> in the vapor phase was considered negligible. This assumption was supported by the fact that equilibrium vapor concentration of 50% w/w H<sub>2</sub>O<sub>2</sub> reactant at 333 K is less than 10% [3]. Additionally, the amount of dissolved O<sub>2</sub> in the liquid was considered negligible compared to the H<sub>2</sub>O<sub>2</sub> and water liquid components, and the amount of water vapor in the gas phase was considered negligible compared to the O<sub>2</sub> gas provided the temperature rise remained below the boiling temperature of water (373 K). The mass balance included the diffusion of H<sub>2</sub>O<sub>2</sub> into liquid water and H<sub>2</sub>O<sub>2</sub>, the bulk flow of the evolving fluid mixture (consisting primarily of liquid H<sub>2</sub>O<sub>2</sub> solution in water, and O<sub>2</sub> gas) down the reactor channel, and consumption of H<sub>2</sub>O<sub>2</sub> resulting from the decomposition reaction. To model the mass balance, the built-in convection and diffusion application mode in the program COMSOL was used. Equation 1 governed the convection and diffusion mass balance of H<sub>2</sub>O<sub>2</sub>.

$$\nabla \cdot (-D_{H_2O_2,eff} \nabla C_{H_2O_2}) + u_s \cdot \nabla C_{H_2O_2} = r_{H_2O_2} \quad (1)$$

In equation 1,  $D_{H_2O_2,eff}$  was the effective diffusivity of H<sub>2</sub>O<sub>2</sub> into the liquid water, H<sub>2</sub>O<sub>2</sub> solution. The diffusivity term neglected diffusion interactions with the catalyst. The mass balance solved for the concentration,  $C_{H_2O_2}$ . The variable  $u_s$  represented the superficial velocity of the fluid. The rate of reaction based on the consumption of hydrogen peroxide,  $r_{H_2O_2}$ , was established assuming first order kinetics weighted via an inputted catalyst mass. The MPB activation energy was set to 20 kJ/mol, whereas the TCC activation was set to 40 kJ/mol. The water and oxygen production rates were related to  $r_{H_2O_2}$ . A conventional Arrhenius relationship defined the reaction rate constant coupling it to the energy balance (equation 2).

Energy Balance. The energy balance of the microreactor system included conduction, advective input and output due to the feed and exit streams, exothermic heat generation due to reaction, sensible heat, and the heat of water vaporization. To model the energy balance, the built-in convection and conduction application mode in COMSOL was used. Equation 2 governed the convection and conduction energy balance.

$$\nabla \cdot (-k_{eff} \nabla T) + u_s c_p \rho \cdot \nabla T = \Delta H_{rxn} r_{H_2O_2} - S_H + \Delta H_{vap} r_{H_2O} \quad (2)$$

In equation 2,  $k_{eff}$  gave the effective thermal conductivity of the reactor channel. The energy balance solved for the variable temperature,  $T$ , coupling it to the mass balance equation. The term,  $u_s$ , still represented the superficial velocity of the fluid. The term  $c_p$  represented heat capacity and the term,  $\rho$ , the average density of the fluid in the microchannel. The heat of reaction,  $\Delta H_{rxn}$ , defined the heat released during the exothermic decomposition reaction. The sensible heat term,  $S_H$ , described the contribution of the heat capacities per product species required to increase the temperature to the boiling point of water. The remaining term of the energy balance,  $\Delta H_{vap}$ , expressed the energy required to vaporize water based on the rate of water production during the reaction.

Momentum Balance. To model the momentum balance, the built-in non-isothermal flow application mode in COMSOL was used. The non-isothermal flow application solves the Navier-Stokes equations for weakly compressible flows (flows with Mach numbers < 0.3). Neglecting the effects of the catalyst in the flow channel and using low initial flow rates maintained the conditions defining weakly compressible fluid flow. The density,  $\rho$ , was modeled as an average of the liquid and gas comprising the fluid weighted by the mole fractions of H<sub>2</sub>O<sub>2</sub>, H<sub>2</sub>O, and O<sub>2</sub> species respectively and changed as the reaction progressed (equation 3).

$$\rho = y_{H_2O_2}\rho_{H_2O_2} + y_{H_2O}\rho_{H_2O} + y_{O_2}\rho_{O_2} \quad (3)$$

In equation 3,  $y_i$  represents the total mole fraction of component  $i$  ( $H_2O_2$ ,  $H_2O$  or  $O_2$ ). This average density was applied under the simplifying assumption that the generated  $O_2$  gas was homogeneously dispersed throughout the effluent liquid. The momentum balance solved for the velocity field giving the superficial velocity of the fluid and the pressure.

### Experimental $H_2O_2$ Decomposition

Effluent oxygen gas rates and temperature data from the MPB experimental microreactor were collected according to the schematic in Figure 2. A syringe or micro - pump was used to dispense thirty or fifty percent  $H_2O_2$  weight in water (30% w/w and 50% w/w) reactant at volumetric flow rates (VFR) from 0.05 ml/min up to 0.15 ml/min. Analogous conditions were used to collect data from the TCC for thermal comparison. The experimental reactor was connected to a water trap system which facilitated the separation of the oxygen gas and liquid product. The  $O_2$  gas proceeded to the oxygen flow meter and the liquid product flowed to the glass collection vial. A NI USB 6008 digital-to-analog converter transmitted the flow data to the laptop for collection and storage. Four thermocouples were placed in 10 mm increments down the length of the MPB reactor channel. A National Instruments USB 9211 digital to analog converter connected to 9162 USB data acquisition device designed specifically to interface with thermocouples transmitted the temperature data to the laptop for temperature data collection and storage. The program Labview Signal Express controlled both the temperature and flow data recording processes.

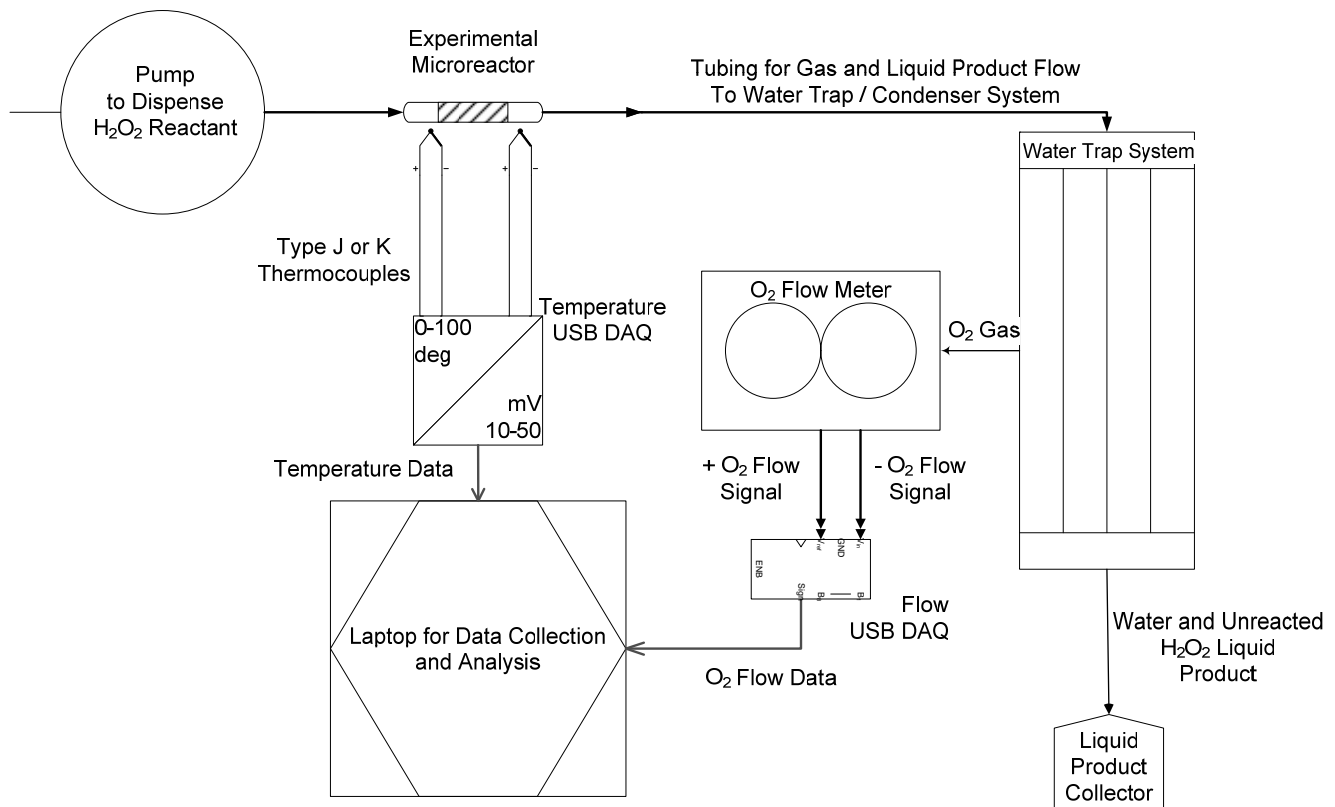
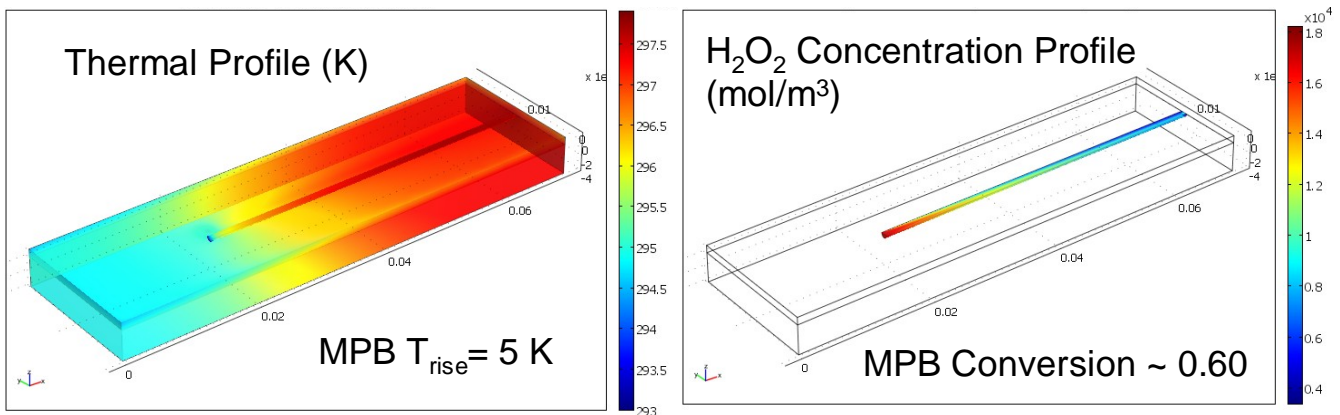


Figure 2: Experimental Setup Schematic

## Results and Discussion

The three-dimensional steady state temperature profile and corresponding  $\text{H}_2\text{O}_2$  concentration profile under the stated conditions for the extended surface area MPB model is shown in Figure 3. Simulations were run to determine which flow rates and concentrations were necessary for 30% or greater conversion given the MPB geometry. The maximum simulated steady state temperature rise for the MPB was less than 10 K for the 50% reactant case with a VFR of 0.15 ml/min, the case that would theoretically generate the greatest heat for the given MPB geometry. Extending the surface areas around the reactor channel further increased the SV ratio of the MPB reactor resulting in enhanced convective cooling, while yielding a simulated steady state conversion greater than 50%. This prompted use of experimental flow rates between 0.05 ml/min and 0.15 ml/min for 50% w/w  $\text{H}_2\text{O}_2$  reactant concentrations. The experimental MPB reactor during a representative decomposition experiment is shown in Figure 4. In the image of the experimental MPB, there is clearly multiphase product in the channel.



Initial Conditions: Reactors with extended surface areas, 50%  $\text{H}_2\text{O}_2$ ,  $8.3\text{e}^{-10} \text{ m}^3/\text{s}$ , MPB: 293 K and Convection Coefficient of  $10 \text{ W}/(\text{m}^2\cdot\text{K})$

Figure 3: Three dimensional temperature and  $\text{H}_2\text{O}_2$  profiles for simulated MPB.

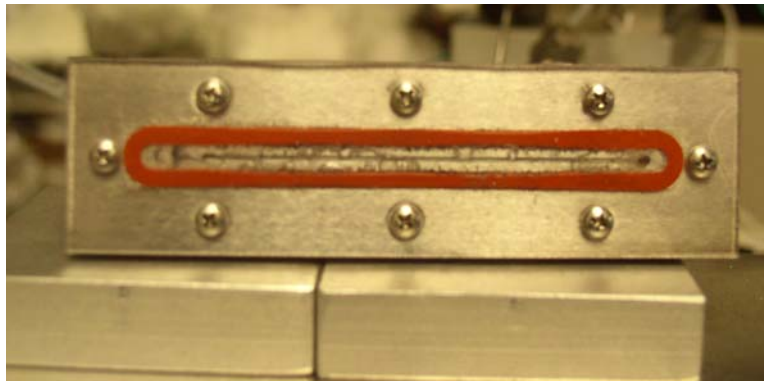
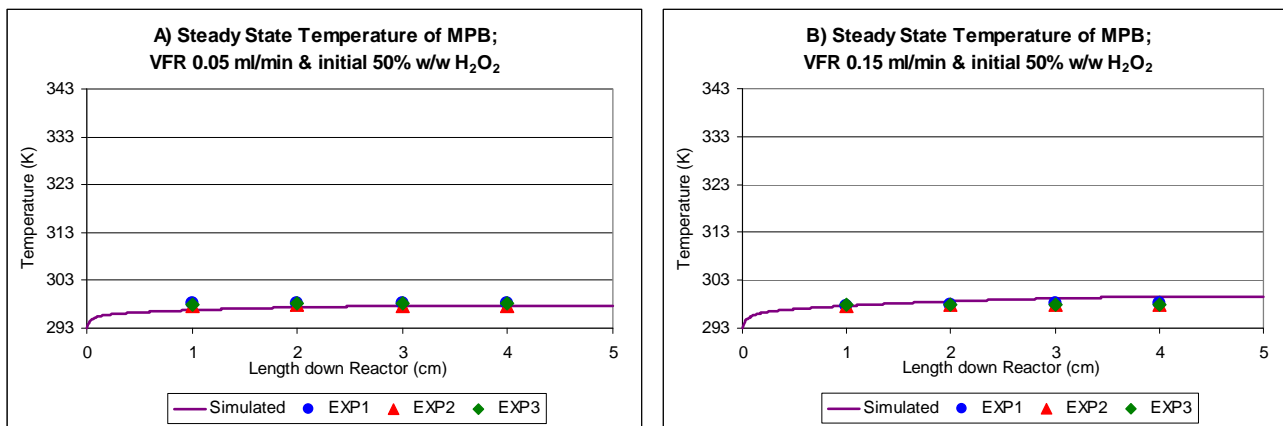


Figure 4: Experimental MPB showing multiphase product stream.

To compare the thermal management of experimental MPB with the simulated MPB, 4 thermocouples recorded temperature at 1, 2, 3, and 4 cm down the length of the experimental MPB. Figures 5A and 5B show the simulated steady state MPB temperature profile versus reactor length given by the solid trend line and the average temperature recordings for 3 experimental runs under steady state operation of the MPB using 50% w/w H<sub>2</sub>O<sub>2</sub> at an initial VFR of 0.05 ml/min and 0.15 ml/min respectively. To compare the thermal management of the MPB with the TCC, 2 thermocouples recorded temperature at 3 and 6.7 cm down the length of the 9.7 cm long TCC reactor. Figures 6A and 6B show the simulated steady state TCC temperature profile versus reactor length given by the solid trend line and the average temperature recordings for representative experimental runs under steady state operation of the TCC using 50% w/w H<sub>2</sub>O<sub>2</sub> at an initial VFR of 0.05 ml/min and 0.15 ml/min respectively.



Figures 5A and 5B: Simulated and recorded steady state MPB temperatures down reactor length for a VFR of A) 0.05 ml/min and B) 0.15 ml/min.

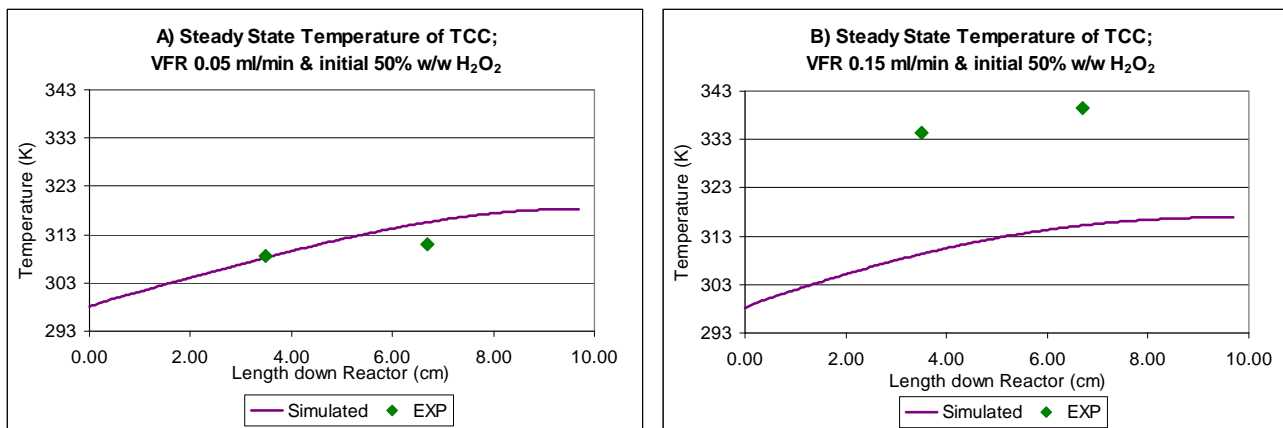


Figure 6A and 6B: Simulated and recorded steady state TCC temperatures down reactor length for a VFR of A) 0.05 ml/min and B) 0.15 ml/min.

Figures 5A and 5B show that the temperature rise was less than 10 K for both the simulated and experimental MPB. Figures 5A and 5B also show that the experimental MPB readings were close to those simulated. However, the experimental MPB data at the higher flow rate had slightly lower temperatures than those simulated. This is likely due to lower experimental conversion compared to the conversion predicted during simulation under the same conditions (Figure 7). When comparing the MPB to the miniature TCC temperatures in Figures 6A and 6B, the MPB shows superior thermal control. Although the TCC exhibited temperature rises less than 100 K, which may be possible with conventionally sized high concentration H<sub>2</sub>O<sub>2</sub> decomposition reactors, it still reached a maximum steady state, experimental temperature of 47 K near the TCC outlet, and was greater than the steady state temperature trend predicted during simulation. This deviation, which was larger at the higher TCC VFR, relates to the break down of the homogenously dispersed, well-mixed assumption used in the modeling and also contributed to the deviation between the simulated and experimental TCC outlet conversions. Although the break down of the well-mixed assumption at the higher VFR affects both the MPB and TCC reactors, the MPB maintained thermal control over the reaction zone, indicating the high MPB SV ratio was successful in mitigating unwanted temperature rise.

Figure 7 depicts the steady state outlet conversions for the MPB and TCC at the stated VFRs using an initial 50% w/w H<sub>2</sub>O<sub>2</sub> and corresponds to the temperature simulations and recordings in Figures 5 and 6 for the given conditions. The highest conversion was observed in the simulated MPB at the lower VFR. This was expected because the lower VFR in the microchannel resulted in the greatest residence time. However, the experimental MPB showed somewhat lower steady state conversion than the simulated values at both flow rates. This decrease in conversion can be explained by the intermittent occupation of catalyst sites by produced oxygen bubbles. These interactions with the catalyst were neglected in the model, but contribute to lower conversions during experimental runs. The TCC run at the higher VFR displays an exception to the mass transfer limitation of oxygen leaving the catalyst sites. In the experimental TCC, distinct slugs of gas and liquid were observed at the outlet, indicating the break down of the well-mixed assumption. The evolution of slug flow in the TCC reactor at the higher VFR probably caused the heat capacity to vary down the reactor channel, permitting the formation of localized hot spots, an increase in reaction, and subsequently higher overall conversion. This result emphasizes the superior control the MPB microreactor has over the prevention of hot spots, and thus the prevention of thermal runaway.

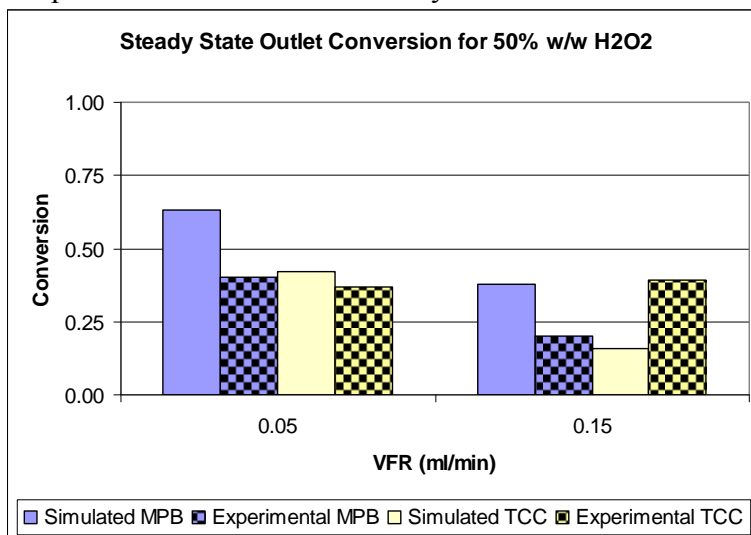


Figure 7: Steady state outlet conversions

## Conclusions

Significant temperature rise (up to 100 K) occurred across a simulated microchannel reactor when the extended surface area was omitted. Increasing the surface-to-volume ratio to enhance passive convective cooling of the simulated MPB facilitated thermal management during catalyzed  $\text{H}_2\text{O}_2$  decomposition. Thermal management was successfully accomplished with the addition of the high area heat exchanger in the simulated MPB reactor, subsequently mitigating the risk of thermal runaway. The momentum balances within the simulated reactors were included under the assumption of homogeneously dispersed oxygen gas in a weakly compressible two-phase fluid to characterize the multiphase effluent product stream. Under this assumption, both the MPB and TCC models demonstrated the promise of thermally controlled  $\text{H}_2\text{O}_2$  decomposition. However when the simulated and experimental data were compared, differences between the simulated and experimental TCC data were large at the higher VFR, indicating the assumption of homogeneously dispersed flow broke down at the higher VFR, especially for the TCC, and the recorded temperature rise was greater than that simulated. Although the divergence of the TCC indicated the break down of the well-mixed assumption at the higher flow rate, and the possible production of hot spots, the consistently small temperature rise (<10K) of the MPB showed the mitigation of thermal runaway even at the higher VFR. However, the observed enhanced thermal control of the MPB may partially result from the temporary occupation of catalyst sites by oxygen gas bubbles, which serves to depress conversion slightly. This possibility is supported by the lower experimental conversions relative to simulated conversion in all cases, except for the TCC at the high VFR, which displayed higher susceptibility to heat effects. Therefore, ways of increasing the conversion via improved catalyst application techniques and the modification of flow dynamics which could dislodge bubbles should be pursued. These findings present a firm foundation for further optimization of thermally controlled  $\text{H}_2\text{O}_2$  decomposition microscale reactors capable of achieving higher conversions, and increased oxygen generation.

## References

- 1 The Navy Unmanned Undersea Vehicle (UUV) Master Plan. In Navy, U.S.D.o.t., ed, pp. 16, 55-58, 67, 702004).
- 2 Salem, I.A.E.-M., Mohamed; Zaki, Ahmed B. Kinetics and Mechanisms of Decomposition Reaction of Hydrogen Peroxide in Presence of Metal Complexes. *International Journal of Chemical Kinetics*, 2000, 32(11), 643-666.
- 3 Bramanti, C.T., L.; Cervone, A.; d'Agostino, L.; Musker, A. J.,; and Saccoccia, G. Experimental Characterization of Advanced Materials for the Catalytic Decomposition of Hydrogen Peroxide. *Proceedings of 42nd AIAA/ASME/ SAE/ASEE Joint Propulsion Conference & Exhibit* Sacramento, CA, USA, 2006).
- 4 Davis, N.S., and Keefe, J.H. Concentrated hydrogen peroxide as a propellant. *Industrial Engineering and Chemistry*, 1956, 48(4), 745-748.
- 5 Papadaki, M., Marqués-Domingo, E., Gao, J. and Mahmud, T. Catalytic decomposition of hydrogen peroxide in the presence of alkylpyridines: Runaway scenarios studies. *Journal of Loss Prevention in the Process Industries*, 2005, 18(4-6), 384-391.
- 6 Guo, J., Jiang, Y. and Al-Dahhan, M.H. Modeling of trickle-bed reactors with exothermic reactions using cell network approach. *Chemical Engineering Science*, 2008, 63(3), 751-764.
- 7 Ehrfeld, W.V.H.H., L., *Microreactors: New Technology for Modern Chemistry*, pp. 5-8 (WILEY-VCH, Weinheim, 2000).
- 8 Jensen, K.F. Microreaction engineering -- is small better? *Chemical Engineering Science*, 2001, 56(2), 293-303.
- 9 Xu, J., Feng, Y. and Cen, J. Transient flow patterns and bubble slug lengths in parallel microchannels with oxygen gas bubbles produced by catalytic chemical reactions. *International Journal of Heat and Mass Transfer*, 2007, 50(5-6), 857-871.